

Energy-Efficient RSMA-enabled Low-altitude MEC Optimization Via Generative AI-enhanced Deep Reinforcement Learning

Xudong Wang, Hongyang Du, Lei Feng, *Member, IEEE*, and Kaibin Huang, *Fellow, IEEE*

Abstract—The growing demand for low-latency computing in 6G is driving the use of UAV-based low-altitude mobile edge computing (MEC) systems. However, limited spectrum often leads to severe uplink interference among ground terminals (GTs). In this paper, we investigate a rate-splitting multiple access (RSMA)-enabled low-altitude MEC system, where a UAV-based edge server assists multiple GTs in concurrently offloading their tasks over a shared uplink. We formulate a joint optimization problem involving the UAV 3D trajectory, RSMA decoding order, task offloading decisions, and resource allocation, aiming to mitigate multi-user interference and maximize energy efficiency. Given the high dimensionality, non-convex nature, and dynamic characteristics of this optimization problem, we propose a generative AI-enhanced deep reinforcement learning (DRL) framework to solve it efficiently. Specifically, we embed a diffusion model into the actor network to generate high-quality action samples, improving exploration in hybrid action spaces and avoiding local optima. In addition, a priority-based RSMA decoding strategy is designed to facilitate efficient successive interference cancellation with low complexity. Simulation results demonstrate that the proposed method for low-altitude MEC systems outperforms baseline methods, and that integrating GDM with RSMA can achieve significantly improved energy efficiency performance.

Index Terms—Rate-Splitting Multiple Access, Mobile Edge Computing (MEC), Resource Allocation, Deep Reinforcement Learning.

I. INTRODUCTION

In the sixth generation (6G) era, the proliferation of Internet of Things (IoT) devices and new immersive applications, such as augmented/virtual reality and holographic telepresence, is driving an unprecedented demand for computational resources at the network edge [1]. These latency-sensitive and computation-intensive services exceed the capabilities of on-board processors in battery-powered ground terminals (GTs), resulting in performance degradation when tasks are executed locally [2]. Mobile edge computing (MEC) offers a viable solution by offloading tasks to proximate edge servers, reducing latency and improving efficiency [2]. However, terrestrial BS-centric MEC is constrained by coverage and capacity, especially in remote or infrastructure-limited environments [3], or when BSs become overloaded or fail to support edge

users. These limitations motivate the exploration of airborne MEC, wherein aerial platforms augment the edge computing infrastructure beyond what ground-based MEC can provide.

In recent years, the low-altitude economy (LAE) has expanded swiftly, with unmanned aerial vehicles (UAVs) emerging as key components in the evolution of mobile communication networks [4], [5]. Dynamically deployed UAVs can form LAE networks that augment terrestrial infrastructure with additional communication and computing capabilities. When equipped with computing units, UAVs serve as airborne MEC servers, enabling low-altitude MEC systems that bring computation offloading closer to users [6]. Such UAV-assisted MEC networks improve coverage and service reliability while significantly reducing end-to-end latency and GT energy consumption, as users no longer need to transmit to distant base stations. Nevertheless, supporting multiple offloading users via a shared UAV radio link introduces substantial multi-user interference. When many users simultaneously offload tasks over limited spectrum resources, interference among their uplink transmissions becomes severe and can drastically bottleneck the system performance, especially under strict bandwidth constraints.

Rate-splitting multiple access (RSMA) has emerged as a promising strategy to manage interference and improve spectral efficiency in multi-user networks [7]. RSMA separates a user's transmission into private and common components, allowing for a combination of interference decoding and noise handling strategies [8]. Unlike uplink Non-Orthogonal Multiple Access (NOMA) with fixed user grouping and power allocation, RSMA offers greater flexibility through adjustable message splits and decoding orders, enhancing spectral efficiency. This makes RSMA well-suited for low-altitude UAV MEC, where multiple GTs can offload concurrently over the shared spectrum without orthogonalization [9]. While existing RSMA studies focus on downlink, extending it to uplink UAV-assisted MEC systems offers new potential for interference mitigation. However, this introduces complex design challenges, requiring joint optimization of UAV trajectory, offloading decisions, RSMA decoding order, and power allocation. Addressing these tightly coupled variables remains a significant challenge.

Conventional optimization techniques, such as convex optimization and heuristic algorithms, are widely used for joint resource and trajectory design but often suffer from high complexity and local optima [10]. Deep reinforcement learning (DRL) offers an online alternative, capable of learning near-

Corresponding author: Lei Feng.

Xudong Wang and Lei Feng are with the State Key Laboratory of Networking and Switching Technology, Beijing University of Posts and Telecommunications, Beijing 100876, China (e-mail: xdwang@bupt.edu.cn; fenglei@bupt.edu.cn).

Hongyang Du and Kaibin Huang are with the Department of Electrical and Electronic Engineering, University of Hong Kong, Pok Fu Lam, Hong Kong SAR, China (e-mail: duhy@eee.hku.hk; huangkb@hku.hk).

optimal policies for joint scheduling and control in high-dimensional environments [11]. However, DRL faces challenges in continuous action spaces, including poor sample efficiency and convergence instability [12]. To address these drawbacks, some studies incorporate generative diffusion models (GDMs), which is a class of generative AI (GenAI) techniques adept at modeling complex distributions through iterative sampling [13]–[16]. By iteratively refining random samples to match an intended distribution, diffusion models excel at generating high-quality solutions even in large search spaces [15]. This motivates our proposed RSMA-assisted low-altitude MEC framework, combining generative AI-enhanced DRL for improved energy efficiency.

A. Related Works

Low-altitude MEC systems are characterized by dynamic node locations, limited computational resources, and a strong dependence on communication link quality, making UAV trajectory planning and computation offloading particularly challenging. As a result, recent studies have investigated the joint optimization of UAV trajectories and resource allocation in low-altitude MEC systems [17]–[20]. For example, the authors in [17] designed a joint task offloading and trajectory control scheme for UAV-assisted energy-harvesting MEC systems to minimize propulsion energy while maintaining queue stability. The authors in [18], [19] proposed joint optimization of communication resources and UAV trajectories to improve offloading throughput or reduce energy consumption under quality of service (QoS) and energy constraints. In [20], a bi-objective ant colony algorithm addressed delay and control cost minimization problem. These studies provide valuable insights into low-altitude edge resource management. However, transmission frameworks based on orthogonal multiple access (OMA) struggle to accommodate the explosive growth in network density, particularly in spectrum-constrained low-altitude networks, often leading to degraded performance in interference management and task completion rates.

Leveraging its capability to mitigate multi-user interference and enhance spectral efficiency, RSMA has been incorporated into low-altitude networks to improve communication performance under interference-limited conditions [21]–[25]. In [21], an alternating optimization strategy for RSMA-enabled low-altitude networks was proposed to maximize system throughput while ensuring user rate requirements. The work in [22] demonstrated that RSMA significantly improves physical-layer security in a dual-UAV downlink scenario. Additionally, RSMA has been introduced into low-altitude MEC systems to further improve offloading performance. Specifically, the authors in [23] designed a UAV relay architecture and propose a data-stream splitting scheme that minimizes UAV energy consumption under task latency constraints. In [24], a joint passive reflecting units and dynamic rate-splitting optimization framework was proposed for uplink RSMA-enabled UAV-MEC systems to minimize total UAV power consumption. The authors in [25] applied RSMA to a UAV-MEC system assisted by a reconfigurable intelligent surface (RIS) with wireless power transfer and observed that

the RSMA-based scheme achieves more reliable and efficient task offloading in the presence of strong co-channel interference. Dynamic low-altitude MEC systems must adapt to time-varying channels and fluctuating interference levels, but traditional iterative optimization methods face scalability challenges when dealing with highly coupled decision variables in such dynamic environments.

Data-driven optimization methods, particularly DRL, have emerged as powerful solutions for complex optimization problems in low-altitude MEC systems due to their dynamic adaptability and global exploration capabilities. For example, the authors in [26] employed DRL to jointly adjust UAV flight paths and offloading decisions, effectively reducing the system's energy consumption and task latency compared to heuristic baselines. To further improve solution quality and avoid local optima, GDMs have been introduced to augment DRL in wireless network optimization [27], [28]. By leveraging the diffusion-based generative process, agents can enhance their exploration of complex state spaces and refine reward evaluation during training [29]–[32]. For instance, the authors in [29] introduced a diffusion-assisted DRL framework that generates diverse state samples and more informative reward signals, achieving faster convergence and lower computational overhead compared to standard DRL in a dynamic resource allocation task. Similarly, in [32], a diffusion-enhanced DRL framework was applied to a wireless sensing-guided edge network to derive optimal pricing strategies, thereby maximizing user utility. Therefore, given the generative capability, integrating diffusion models with DRL to address joint trajectory and resource allocation in RSMA-enabled low-altitude MEC systems presents a promising research direction.

B. Motivations and Contributions

This paper presents a joint optimization framework for uplink RSMA-enabled low-altitude MEC systems to maximize energy efficiency. We proposed a GenAI-enhanced DRL algorithm to jointly optimize UAV trajectory, user offloading, RSMA decoding order, and power allocation. By embedding a GDM generator into the DRL agent, the proposed algorithm effectively explores complex solution spaces and mitigates local optima issues common in conventional approaches. The main contributions are summarized as follows:

- We develop a uplink RSMA-assisted low-altitude MEC system, where a UAV equipped with an mobile edge server provides computing services to multiple GTs, and the task data of each GT is split into multiple sub-messages that are concurrently transmitted with different powers. Then we formulate a novel non-convex optimization problem that maximizes energy efficiency by jointly optimizing the UAV's flight trajectory, user offloading decisions, and RSMA communication parameters.
- We propose a generative AI-enhanced deep reinforcement learning framework, termed GDRS, to efficiently solve the high-dimensional, non-convex optimization problem in RSMA-enabled UAV-MEC systems. The problem is decomposed into a decoding-order sub-problem and a continuous control problem. To reduce the decoding

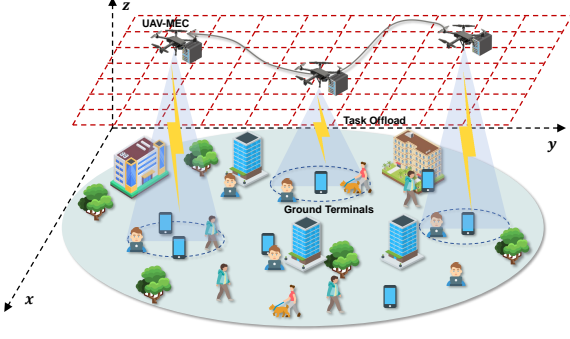


Fig. 1. RSMA-enabled multi-user low-altitude MEC networks.

complexity, we derive a lightweight priority-based RSMA strategy that dynamically orders sub-messages based on channel quality and user QoS demands, enabling interference cancellation with low overhead.

- To overcome the challenges of poor exploration and local optima, we embed a generative diffusion model into the policy network. This integration allows the agent to generate structured candidate actions, including UAV trajectories and resource allocation decisions, leading to more stable convergence and higher policy quality across dynamic and coupled state-action spaces.
- We carried out a comprehensive set of simulations to validate the proposed GDRS and to assess the scalability of the RSMA framework. The results show that our RSMA-enabled framework achieves higher throughput and energy efficiency compared to NOMA-based schemes. Moreover, the GenAI-enhanced DRL method outperforms conventional DRL approaches in terms of reward, highlighting the superior exploration capability of the diffusion model.

The rest of this paper is organized as follows. Section II introduces the system model and formally defines the optimization problem. In Section III, we elaborate on the algorithmic framework developed to address the problem. Section IV showcases simulation results and provides an in-depth discussion of the numerical findings. Section V highlights the key contributions and draws the final conclusions of the paper.

II. SYSTEM MODEL AND PROBLEM FORMULATION

As illustrated in Fig. 1, we investigate an RSMA-assisted low-altitude MEC systems, where the UAV is despatched to serve $\mathcal{K} \triangleq \{1, 2, \dots, K\}$ GTs.

A. Network Model

The task area is partitioned into a grid of cells with identical area. The horizontal coordinate of the center of the i -th cell is represented by $D_i^\ell = [x_i, y_i]^T \in \mathbb{R}^{2 \times 1}$, where $\mathcal{L} \triangleq \{1, 2, \dots, L\}$ denotes the set of all cell indices. The spacing between the centers of neighboring cells along the x -axis and y -axis are denoted by x_s and y_s , respectively. The UAV's horizontal position is represented by $D_n^u \in \mathcal{L}$, where $n \in \mathcal{N} \triangleq \{1, 2, \dots, N\}$ and N represents the total number of discrete time slots. Each time slot is associated with a

UAV flight duration level $t_n^u \in \mathcal{T} \triangleq \{1, 2, \dots, T\}$, where the actual duration is bounded by $t_{\min} \leq t_n^u \times \Delta t \leq t_{\max}$. Here, t_{\min} and t_{\max} define the minimum and maximum allowable flight durations, and $\Delta t = \lfloor t_{\max}/T \rfloor$ denotes the time resolution per level. The initial and final UAV positions are fixed and denoted as D_0^u and D_e^u , respectively. Accordingly, the horizontal UAV path can be approximated as the sequence $\{D_0^u, D_1^u, \dots, D_n^u, \dots, D_N^u, D_e^u\}$. To capture the UAV's vertical mobility, the altitude at time slot n is represented by $h_n^u \in \mathcal{H} \triangleq \{1, 2, \dots, H\}$. The actual height must satisfy $h_{\min} \leq h_n^u \times \Delta h \leq h_{\max}$, where h_{\min} and h_{\max} denote the minimum and maximum permissible heights, respectively, and $\Delta h = \lfloor h_{\max}/H \rfloor$ denotes the step size between discrete altitude levels. Consequently, the complete UAV trajectory consists of N discrete 3D waypoints $[D_n^u, h_n^u]$ and the associated time durations $t_n^u, \forall n \in \mathcal{N}$.

B. Mobility Model

In UAV-assisted MEC systems, GTs are typically either stationary or exhibit low mobility. Thus, the position of each GT is assumed to be known a priori and represented by $u_k = [x_k, y_k]^T \in \mathbb{R}^{2 \times 1}, k \in \mathcal{K}$ throughout the entire operation period. The horizontal velocity of UAV is expressed as

$$v_n^h = \frac{\|D_{n+1}^u - D_n^u\|}{t_n^u} \leq V_{\max}^h, \forall n \in \mathcal{N}, \quad (1)$$

where V_{\max}^h represents the maximum horizontal velocity. Besides, the vertical flying velocity is expressed as

$$v_n^v = \frac{\|h_{n+1}^u - h_n^u\|}{t_n^u} \leq V_{\max}^v, \forall n \in \mathcal{N}, \quad (2)$$

where V_{\max}^v denotes the UAV's maximum vertical velocity. When $v_n^h = 0$, the UAV is either hovering or performing steady straight-and-level flight during time slot n .

Based on [33], the propulsion energy consumption of the UAV is given by

$$E^{\text{uav}} = \sum_{n=1}^N t_n^u \left(W_0 \left(1 + \frac{3(v_n^h)^2}{U_t^2} \right) + \frac{1}{2} F_0 \rho g M (v_n^h)^3 + W_1 \left(\sqrt{1 + \frac{(v_n^h)^4}{4\bar{v}^4}} - \frac{(v_n^h)^2}{2\bar{v}^2} \right)^{\frac{1}{2}} + W_2 v_n^v \right), \quad (3)$$

where W_0 and W_1 represent the constant blade profile power and the induced power under hovering conditions, while W_2 denotes the constant power required during ascent or descent. The parameters F_0 and g represent the fuselage drag ratio and the rotor solidity. In addition, ρ refers to the air density, and M stands for the area of the rotor disc. The parameter U_t denotes the tip velocity of the rotor blade, and \bar{v} signifies the tip velocity of the rotor blade, and \bar{v} refers to the average induced airflow velocity in hovering flight.

C. Communication Model

Based on the air-to-ground propagation model for urban scenarios [34], the probability of establishing the LoS connection between the UAV and GT k can be expressed as

$$J_{k,n} = \frac{1}{1 + \alpha \exp \left(-\beta \left(\arctan \left(\frac{h_n^u}{l_{k,n}} \right) - \alpha \right) \right)}, \quad (4)$$

where α and β are environment-dependent constants, $l_{k,n} = \sqrt{(x_i - x_k)^2 + (y_i - y_k)^2}$. Based on this, the corresponding pathloss can be expressed as

$$d_{k,n} = 20\log\left(\sqrt{(h_n^u)^2 + l_{k,n}^2}\right) + A_1 \times j_{k,n} + A_2, \quad (5)$$

where $A_1 = \zeta_{\text{LoS}} - \zeta_{\text{NLoS}}$, $A_2 = 20\log(\frac{4\pi f_c}{c}) + \zeta_{\text{NLoS}}$, f_c denotes the carrier frequency; c represents the speed of light, ζ_{LoS} and ζ_{NLoS} are the environment-dependent path loss factors for LoS and NLoS conditions, respectively. We define $a_{k,n} \in \{0, 1\}$ as the offloading indicator of GT k at time slot n , with $a_{k,n} = 1$ representing task offloading to the UAV and $a_{k,n} = 0$ indicating local computation. To support concurrent offloading, RSMA is applied. Specifically, the message of each GT $w_{k,n}$ is split into $|\mathcal{I}|$ sub-messages $w_{k,n,i}$, each allocated a transmit power $p_{k,n,i}$ to achieve rate splitting, such that $\sum_{i \in \mathcal{I}} p_{k,n,i} \leq P_{\max}, \forall k, n$, where P_{\max} is the maximum uplink transmit power of each GT. The composite message is $w_{k,n} = \sum_{i \in \mathcal{I}} \sqrt{p_{k,n,i}} w_{k,n,i}, \forall k, n$. Thus, the received signal of UAV at time slot n is obtained as

$$\begin{aligned} y_n &= \sum_{k \in \mathcal{K}} a_{k,n} \sqrt{g_{k,n}} w_{k,n} + n_0 \\ &= \sum_{k \in \mathcal{K}} a_{k,n} \sum_{i \in \mathcal{I}} \sqrt{g_{k,n} p_{k,n,i}} w_{k,n,i} + n_0, \end{aligned} \quad (6)$$

where $g_{k,n}$ denotes the channel gain between k -th GT and UAV, given by $g_{k,n} = 10^{-d_{k,n}/10}$, where n_0 represents the additive white Gaussian noise (AWGN). To decode multiple sub-messages, the UAV employs successive interference cancellation (SIC). Let $\pi_{k,n,i}, i \in \mathcal{I}$ indicate the SIC decoding order of sub-message $w_{k,n,i}$, and let $\pi = \{\pi_{k,n,i}, \forall k, n, i\}$ denote a decoding permutation, which contains all valid SIC decoding sequences for the $|\mathcal{I}| K$ sub-messages. Under this decoding strategy, the achievable uplink rate for sub-message $w_{k,n,i}$ is obtained as [24]

$$R_{k,n,i} = B \log_2 \left(1 + \frac{g_{k,n} p_{k,n,i}}{BN_0 + \sum_{(k',i') \in \mathcal{W}_{k,n,i}} g_{k',n} p_{k',n,i'}} \right), \quad (7)$$

where B denotes the system bandwidth, N_0 represents the noise power spectral density. The set $\mathcal{W}_{k,n,i} = \{(k', i') | a_{k',n} = a_{k,n}, \pi_{k',n,i'} > \pi_{k,n,i}, \forall k', i'\}$ contains the sub-messages that are decoded after $w_{k,n,i}$ based on the SIC decoding order at the UAV.

D. Computing Model

In the considered RSMA-enabled low-altitude MEC systems, each GT has an estimated computational task $G_k = \{C_k, D_k\}$, where C_k represents the total required CPU cycles, D_k denotes the overall data size to be calculated. As discussed in [35], when GT k chooses to offload its task to the UAV during time slot n , the expected amount of data successfully transmitted in that slot is obtained as

$$m_{k,n} = \sum_{i \in \mathcal{I}} a_{k,n} \kappa_n t_n^u R_{k,n,i}, \quad (8)$$

where $\kappa_n \in [0, 1]$ represents the portion of time slot n that is assigned to data transmission. To ensure that the transmitted

data $m_{k,n}$ can be processed by the UAV's onboard CPU with a processing rate of f_u , κ_n must be properly chosen. This requirement imposes the following constraint:

$$\sum_{i \in \mathcal{I}} \kappa_n t_n^u R_{k,n,i} \leq f_u (1 - \kappa_n) t_n^u \frac{D_k}{C_k}. \quad (9)$$

To further enhance the total amount of processed data, α_n is further constrained as

$$\kappa_n = \frac{f_u D_k}{\sum_{i \in \mathcal{I}} R_{k,n,i} C_k + f_u D_k}. \quad (10)$$

Given the offloading decision $a_{k,n}$ at time slot n and (10), the amount of task data G_k processed during slot n is represented as

$$\varpi_{k,n} = a_{k,n} \frac{f_u D_k t_n^u \sum_{i \in \mathcal{I}} R_{k,n,i}}{\sum_{i \in \mathcal{I}} R_{k,n,i} C_k + f_u D_k} + (1 - a_{k,n}) t_n^u f_g, \quad (11)$$

where f_g denotes the processing speed of the GT's CPU. In (11), the delay due to downlink transmission from UAV to GT is neglected, assuming that the corresponding data size is negligible. Accordingly, the overall system energy efficiency can be defined as $\eta = \sum_{k=1}^K \sum_{n=1}^N \varpi_{k,n} / E^{\text{uav}}$.

E. Problem Formulation

We aim to maximize the system energy efficiency η while maintaining reliable MEC performance by jointly optimizing the UAV trajectory, task offloading decisions, uplink power allocation, and SIC decoding order. Let $\mathbf{A} = \{a_{k,n}, \forall k \in \mathcal{K}, \forall n \in \mathcal{N}\}$, $\mathbf{P} = \{p_{k,n,i}, \forall k \in \mathcal{K}, \forall n \in \mathcal{N}, \forall i\}$, $\mathbf{D} = \{D_n^u, \forall n \in \mathcal{N}\}$, $\mathbf{h} = \{h_n^u, \forall n \in \mathcal{N}\}$, and $\mathbf{t} = \{t_n^u, \forall n \in \mathcal{N}\}$, the optimization problem can then be formulated as

$$\mathcal{P}0 : \max_{\mathbf{A}, \mathbf{P}, \mathbf{D}, \mathbf{h}, \mathbf{t}, \pi} \eta \quad (12a)$$

$$\text{s.t. } C1 : a_{k,n} = \{0, 1\}, \forall k \in \mathcal{K}, \forall n \in \mathcal{N}, \quad (12b)$$

$$C2 : \sum_{n \in \mathcal{N}} \varpi_{k,n} \geq D_k, \forall k \in \mathcal{K}, \quad (12c)$$

$$C3 : \sum_{i \in \mathcal{I}} p_{k,n,i} \leq P_{\max}, \forall k \in \mathcal{K}, \forall n \in \mathcal{N}, \quad (12d)$$

$$C4 : \frac{\|D_{n+1}^u - D_n^u\|}{t_n^u} \leq V_{\max}^h, \forall n \in \mathcal{N}, \quad (12e)$$

$$C5 : \frac{\|h_{n+1}^u - h_n^u\|}{t_n^u} \leq V_{\max}^v, \forall n \in \mathcal{N}, \quad (12f)$$

$$C6 : h_{\min} \leq h_n^u \times \Delta h \leq h_{\max}, \forall n \in \mathcal{N}, \quad (12g)$$

$$C7 : t_{\min} \leq t_n^u \times \Delta t \leq t_{\max}, \forall n \in \mathcal{N}, \quad (12h)$$

$$C8 : p_{k,n,i} \geq 0, \forall k \in \mathcal{K}, \forall n \in \mathcal{N}, \forall i \in \mathcal{I}, \quad (12i)$$

$$C9 : \pi \in \Pi, \quad (12j)$$

$$C10 : \sum_{i \in \mathcal{I}} R_{k,n,i} \geq R_{\min}, \forall k \in \mathcal{K}, \forall n \in \mathcal{N} \quad (12k)$$

$$C11 : R_{k,n,1} : R_{k,n,2} : \dots : R_{k,n,I} = \mu_{k,n,1} : \mu_{k,n,2} : \dots : \mu_{k,n,I}, \forall k \in \mathcal{K}, \forall n \in \mathcal{N}, \quad (12l)$$

where $\mu_{k,n,i}$ denotes a predefined non-negative coefficient that allocates a proportion of the rate $R_{k,n}$ to the i -th sub-message of GT k in time slot n , satisfying $R_{k,n,i} = \mu_{k,n,i} R_{k,n}, \forall i$ and $\sum_{i \in \mathcal{I}} \mu_{k,n,i} = 1, \forall k, n$. The minimum rate requirement for

each GT is denoted by R_{\min} . Constraints in $\mathcal{P}0$ are interpreted as follows: C1 models offloading as a binary decision problem; C2 ensures tasks are completed within the UAV's mission time; C3 limits the total transmit power of each GT; C4 ~ C7 describe UAV mobility constraints; C8 enforces non-negative transmission powers; C9 guarantees feasible SIC decoding; C10 enforces the rate requirement; and C11 ensures valid rate splitting among sub-messages.

The optimization problem $\mathcal{P}0$ is a non-convex mixed-integer program due to the discrete offloading variable \mathbf{a} , the non-convex objective, and constraint C2, making it difficult to solve optimally. Moreover, the UAV's complex energy model further complicates trajectory and flight time design for energy efficiency maximization. Prior work has shown that solving $\mathcal{P}0$ via successive convex approximation (SCA) incurs high computational cost, rendering it impractical [33]. To overcome these challenges, we derive the optimal decoding order policy, and then develop a GenAI-based optimization framework, detailed in the following section.

III. THE PROPOSED GDRS ALGORITHM

To efficiently address problem $\mathcal{P}0$, we decompose it into two sub-problems: 1) the decoding order sub-problem $\mathcal{P}1$, and 2) the joint UAV 3D trajectory, power allocation, and task offloading sub-problem $\mathcal{P}2$. For $\mathcal{P}1$, the optimal decoding policy π is determined based on channel gains. Subsequently, $\mathcal{P}2$ is reformulated as a Markov decision process (MDP), and a generative AI-enhanced DRL framework is developed to optimize $\{\mathbf{A}, \mathbf{P}, \mathbf{D}, \mathbf{h}\}$.

A. Decoding Order Policy

The optimal decoding order plays a critical role in mitigating inter-submessage interference and enhancing overall energy efficiency, and thus must be carefully considered. Given a fixed UAV trajectory \mathbf{D} , altitude profile \mathbf{h} , offloading decisions \mathbf{A} , power allocation \mathbf{P} , and UAV flight time \mathbf{t} , $\mathcal{P}0$ is rewritten as

$$\mathcal{P}1 : \max_{\pi} \eta \quad (13a)$$

$$\text{s.t. C9, C10, C11.} \quad (13b)$$

Solving the decoding order optimization problem $\mathcal{P}1$ is challenging due to its non-convex objective function and the intricate interdependence of discrete variables, rendering it a mixed-integer nonlinear programming (MINLP) problem that is typically hard to solve. While exhaustive search methods [36] can yield the optimal solution, their computational cost scales exponentially with the number of sub-messages, making them impractical for multi-user systems. Existing works [37]–[39] often adopt channel gain-based heuristics for decoding order. To better balance computational efficiency and system performance, we propose a decoding strategy that jointly considers both the channel gains and the rate-splitting proportions of each GT's sub-messages.

Proposition 1. *The decoding order of sub-messages is determined by sorting $v_{k,n,i} \triangleq |g_{k,n}|^2 \left(1 + \frac{1}{\rho_{k,n,i}^{\min}}\right) =$*

$|g_{k,n}|^2 \left(1 + \frac{1}{2^{(\mu_{k,n,i} R_{\min})} - 1}\right)$ in descending order, where $\rho_{k,n,i}^{\min}$ represents the minimum signal-to-interference-plus-noise ratio (SINR) required for GT k to decode the i -th sub-message at time slot n .

Proof. Since the decoding order policy π influences the achievable data rate but does not impact the energy consumption of UAV, the optimization problem $\mathcal{P}1$ is equivalently reformulated as

$$\mathcal{P}1.1 : \max_{\pi_{k,n,i}} \sum_{k \in \mathcal{K}} \varpi_{k,n} \quad (14a)$$

$$\text{s.t. C9, C10, C11.} \quad (14b)$$

As indicated in (11), for given UAV trajectory \mathbf{D} , altitude profile \mathbf{h} , offloading decisions \mathbf{A} , power allocation \mathbf{P} , and flight time \mathbf{t} , the data processed $\varpi_{k,n}$ depends solely on the sum rate $\sum_{i \in \mathcal{I}} R_{k,n,i}$. Hence, maximizing $\varpi_{k,n}$ reduces to maximizing the aggregate rate. To this end, we aim to design a decoding order policy that maximizes the sum rate at each time slot. Let w_a and w_b be two consecutive sub-messages in the decoding sequence, associated with respective channel gains g_a and g_b , and corresponding power levels p_a and p_b . If the cumulative interference from previously decoded sub-messages is upper bounded by a constant ϵ , we have

$$|g_a|^2 p_a + |g_b|^2 p_b + \xi + N_0 \leq \epsilon, \quad (15)$$

where ξ represents the interference from sub-messages decoded after both w_a and w_b . Two decoding scenarios are possible: a) w_a is decoded before w_b , and b) w_b is decoded before w_a . We analyze the achievable signal strength under both cases. Case a): when w_a decoded first: In Case a), where w_a is decoded first, the feasible power allocation for w_a and w_b must satisfy

$$\frac{|g_a|^2 p_a}{|g_b|^2 p_b + \xi + N_0} \geq \rho_a^{\min}, \quad \frac{|g_b|^2 p_b}{\xi + N_0} \geq \rho_b^{\min}, \quad (16)$$

where $0 \leq p_a, p_b \leq P_{\max}$. Based on this feasible region, the corresponding lower bound of the achievable signal strength can be expressed as

$$p_a \geq \frac{\rho_a^{\min}(\rho_b^{\min} + 1)(\xi + N_0)}{|g_a|^2}, \quad p_b \geq \frac{\rho_b^{\min}(\xi + N_0)}{|g_b|^2}, \quad (17)$$

and the associated upper limit for power control is given by

$$p_a \leq P_{\max}, \quad p_b \leq \min \left\{ P_{\max}, \frac{\frac{|g_a|^2 P_{\max}}{\rho_a^{\min}} - \xi - N_0}{|g_b|^2} \right\}, \quad (18)$$

The maximum achievable signal strength from sub-messages w_a and w_b , denoted by $\chi \triangleq |g_a|^2 p_a + |g_b|^2 p_b$, can thus be written as

$$\chi \leq \chi_a \triangleq \min \left\{ |g_a|^2 P_{\max} \left(1 + \frac{1}{\rho_b^{\min}}\right), \right. \\ \left. (|g_a|^2 + |g_b|^2) P_{\max}, \epsilon - \xi - N_0 \right\}. \quad (19)$$

Case b): when w_b is decoded first, the maximum combined signal strength from w_a and w_b can similarly be expressed as

$$\chi \leq \chi_b \triangleq \min \left\{ |g_b|^2 P_{\max} \left(1 + \frac{1}{\rho_b^{\min}} \right), \right. \\ \left. (|g_a|^2 + |g_b|^2) P_{\max}, \epsilon - \xi - N_0 \right\}. \quad (20)$$

By comparing expressions (19) and (20), we observe that in Case a), if $|g_a|^2 \left(1 + \frac{1}{\rho_a^{\min}} \right) \geq |g_b|^2 \left(1 + \frac{1}{\rho_b^{\min}} \right)$, then $\chi_a \geq \chi_b$, i.e., decoding of w_a , indicating that decoding w_a first yields higher signal strength. Conversely, in Case b), if $|g_a|^2 \left(1 + \frac{1}{\rho_a^{\min}} \right) \leq |g_b|^2 \left(1 + \frac{1}{\rho_b^{\min}} \right)$, then $\chi_a \leq \chi_b$, and decoding w_b first becomes the better choice.

This confirms that the optimal decoding strategy is to prioritize decoding the sub-message $w_{k,n,i}$ corresponding to the larger value of $|g_{k,n}|^2 \left(1 + \frac{1}{\rho_{k,n,i}^{\min}} \right)$. Accordingly, a near-optimal decoding order is obtained by sorting all sub-messages in descending order of $v_{k,n,i} \triangleq |g_{k,n}|^2 \left(1 + \frac{1}{\rho_{k,n,i}^{\min}} \right) = |g_{k,n}|^2 \left(1 + \frac{1}{2^{(\mu_{k,n,i} R_{\min}) - 1}} \right)$. This concludes the proof. \square

B. MDP Construction

With the decoding order strategy π determined, problem P0 is reformulated as

$$\mathcal{P}2: \max_{\mathbf{A}, \mathbf{P}, \mathbf{D}, \mathbf{h}, \mathbf{t}} \eta \quad (21a)$$

$$\text{s.t. C1} \sim \text{C8}. \quad (21b)$$

To obtain the optimal joint trajectory, task offloading, and power allocation, we propose generative AI-enhanced DRL method.

DRL operates on two core components: the agent and the environment. Their interaction is typically modeled as a MDP, characterized by $\langle \mathcal{S}, \mathcal{A}, \mathcal{R}, \omega, \mathcal{P} \rangle$, where \mathcal{S} denotes the state space, and \mathcal{A} the action space available to the agent. The reward function \mathcal{R} quantifies the immediate feedback received after taking a specific action in a particular state, whereas the discount factor ω controls the trade-off between short-term and long-term rewards. The transition probability function \mathcal{P} governs the dynamics of state evolution following each action. The key components \mathcal{S} , \mathcal{A} , and \mathcal{R} are detailed as follows:

1) *State Spaces*: At time slot n , the state of GT k is defined by its fixed location, i.e., $s_k(n) = u_{kn} \triangleq u_k, \forall n \in \mathcal{N}$. The state of UAV $s_u(n)$ can be represented by its 3D position and time allocation, i.e., $s_u(n) = (D_n^u, h_n^u, t_n^u)$. Hence, the overall system state at slot n is obtained as $s(n) = \{\{s_k(n)\}_{k \in \mathcal{K}}, s_u(n), n\} \in \mathcal{S}$.

2) *Action Spaces*: Following the mobility model in [40], the UAV is allowed to move only to one of the adjacent horizontal cells within a single time slot. As a result, its horizontal position $D_u(n)$ is updated in the next slot as:

$$D_u(n+1) = \begin{cases} D_u(n) + (0, y_s), & \text{if } d(n) = N \\ D_u(n) - (0, y_s), & \text{if } d(n) = S \\ D_u(n) + (x_s, 0), & \text{if } d(n) = E \\ D_u(n) - (x_s, 0), & \text{if } d(n) = W \\ D_u(n) + (0, 0), & \text{if } d(n) = I \end{cases} \quad (22)$$

where $d(n)$ denotes the UAV's selected horizontal flight action at time slot n , with E, S, W , and N , indicating movement in the directions of east, south, west, and north, respectively. The symbol I signifies the UAV remains stationary. In the vertical dimension, the UAV is similarly constrained to move only to an adjacent altitude level in each time slot. Accordingly, the UAV's altitude h_n^u will be updated in the next slot as:

$$h_{n+1}^u = \begin{cases} h_n^u + 1, & \text{if } h(n) = U \\ h_n^u - 1, & \text{if } h(n) = D \\ h_n^u + 0, & \text{if } h(n) = I \end{cases} \quad (23)$$

where $h(n)$ denotes the UAV's chosen altitude action at time slot n ; U and D represent ascending and descending, respectively. If the selected horizontal action $d(n)$ leads the UAV outside the area of interest at time slot $n+1$, it is reset to I to keep the UAV stationary. Similarly, if $h(n)$ causes the UAV's altitude to exceed the allowable range $[h_{\min}, h_{\max}]$, it is set to I to retain the current altitude level. Accordingly, the system action at time slot n can be expressed as $a(n) = (d(n), h(n), t_n^u, \{a_{k,n}\}_{k \in \mathcal{K}}, \{p_{k,n,i}\}_{k \in \mathcal{K}, i \in \{1,2\}}) \in \mathcal{A}$, where the action space \mathcal{A} comprises the UAV's movement and time allocation actions, as well as the GTs' task offloading and power control decisions.

3) *Rewards*: The reward associated with a state-action pair $(s(n), a(n))$ at time slot n is given by:

$$r(s(n), a(n)) = \lambda_1 \sum_{k \in \mathcal{K}} \frac{\varpi_{k,n+1}}{E_{n+1}^{\text{uav}}} - \lambda_2 PV. \quad (24)$$

After performing action $a(n)$, the reward $r(s(n), a(n))$ is defined as the energy efficiency, measured by the ratio between the amount of data processed by each GT in the next time slot, i.e., $\varpi_{k,n+1}$, and the UAV's propulsion energy consumption E_{n+1}^{uav} . To influence the convergence behavior, two scaling factors λ_1 and λ_2 are introduced. Additionally, PV denotes a penalty function, which is defined as

$$PV = \begin{cases} c_0, & \text{if C1} \sim \text{C8 are not satisfied,} \\ 0, & \text{Otherwise,} \end{cases} \quad (25)$$

where c_0 is a positive constant that controls the penalty magnitude. Through this design, the DRL framework aims to learn energy-efficient solutions for RSMA-enabled low-altitude MEC systems.

C. The Proposed Generative AI-enhanced DRL Method

Jointly optimizing UAV trajectory, task offloading, and power allocation presents significant challenges for conventional DRL algorithms, primarily due to the high-dimensional and discrete nature of the action space. Standard DRL agents often exhibit poor sample efficiency and limited exploration capability under such structured constraints. To address these issues, we adopt a diffusion model-based DRL framework that utilizes generative modeling via a learned denoising process to generate structured actions. This method promotes more efficient exploration and supports the synthesis of valid, high-quality policies that better satisfy system constraints and optimize long-term energy efficiency.

The Denoising Diffusion Probabilistic Model (DDPM) progressively perturbs data into Gaussian noise through a forward diffusion process and then learns to recover the original data via a reverse denoising process [41]. Leveraging this generative mechanism and its ability to incorporate conditional information, we design a diffusion-based optimizer for enhancing solution quality and synergizing effectively with DRL to address dynamic and complex optimization in RSMA-enabled low altitude MEC systems.

In the diffusion framework, an optimal decision under the current environment is progressively perturbed with noise until it becomes Gaussian, a process referred to as forward probability noising [13]. In the reverse phase, the decision generation network $\pi_\theta(\cdot)$ serves as a denoiser that reconstructs the original solution z_0 from Gaussian noise, conditioned on the system state s . The following presents the formal mathematical formulation of this diffusion-based decision process.

1) *Forward Process*: The decision output $z_0 = \pi_\theta(s)$ represents the probability distribution over discrete decisions under the observed environment state s . In the forward diffusion process, this initial distribution is gradually perturbed by Gaussian noise, resulting in a sequence of intermediate representations z_1, z_2, \dots, z_T , each sharing the same dimensionality as z_0 . At each step t , the transition from z_{t-1} to z_t follows a Gaussian distribution with mean $\sqrt{1 - \varphi_t} z_{t-1}$ and variance $\varphi_t \mathbf{I}$, as described in [42].

$$q(z_t|z_{t-1}) = \mathcal{N}(z_t; \sqrt{1 - \varphi_t} z_{t-1}, \varphi_t \mathbf{I}), \quad (26)$$

where $t = 1, \dots, T$, $\varphi_t = 1 - e^{-\frac{\varphi_{\min}}{T} - \frac{2t-1}{2T^2}(\varphi_{\max} - \varphi_{\min})}$ denotes the time-dependent variance in the forward process [42].

Since each z_t depends only on its immediate predecessor z_{t-1} , the forward process constitutes a Markov chain. Consequently, the distribution of z_T conditioned on z_0 can be expressed as the product of transition probabilities across denoising steps [42], which is shown as

$$q(z_T|z_0) = \prod_{t=1}^T q(z_t|z_{t-1}). \quad (27)$$

Although the forward process is not explicitly executed, it defines a closed-form relationship between z_0 and any intermediate state z_t , given by

$$z_t = \sqrt{\bar{\nu}_t} z_0 + \sqrt{1 - \bar{\nu}_t} \epsilon, \quad (28)$$

where $\nu_t = 1 - \varphi_t$, $\bar{\nu}_t = \prod_{k=1}^t \nu_k$ denotes the cumulative product up to step t . The forward process relates z_t and z_0 as a noisy transformation, where $\epsilon \sim \mathcal{N}(\mathbf{0}, \mathbf{I})$ is standard Gaussian noise. As t increases, z_T converges to pure noise distributed as $\mathcal{N}(\mathbf{0}, \mathbf{I})$. However, since wireless network optimization problems typically lack ground-truth datasets of optimal decisions z_0 , the forward process is not executed in the proposed framework.

2) *Reverse Process*: The goal of the reverse process is to reconstruct the desired target z_0 starting from a noise sample $z_T \sim \mathcal{N}(\mathbf{0}, \mathbf{I})$ by iteratively denoising it. Within our framework, this procedure corresponds to synthesizing the optimal decision policy from an initially Gaussian-distributed sample. The transition between z_t and z_{t-1} is modeled as

$p(z_{t-1}|z_t)$, which is intractable in closed form but can be approximated by a Gaussian distribution, expressed as

$$p_\theta(z_{t-1}|z_t) = \mathcal{N}(z_{t-1}; \mu_\theta(z_t, t, s), \tilde{\varphi}_t \mathbf{I}), \quad (29)$$

where the mean μ_θ is learned via a deep neural network, and the variance is obtained as [42].

$$\tilde{\varphi}_t = \frac{1 - \bar{\nu}_{t-1}}{1 - \bar{\nu}_t} \varphi_t \quad (30)$$

By applying Bayes' theorem, the reverse process can be reformulated in terms of the forward process and expressed as a Gaussian probability density function. Accordingly, the mean is derived as

$$\mu_\theta(z_t, t, s) = \frac{\sqrt{\bar{\nu}_t}(1 - \bar{\nu}_{t-1})}{1 - \bar{\nu}_t} z_t + \frac{\sqrt{\bar{\nu}_{t-1}} \varphi_t}{1 - \bar{\nu}_t} z_0, \quad (31)$$

where $t = 1, \dots, T$. Based on the forward process in (28), the reconstructed sample z_0 can be directly estimated by

$$z_0 = \frac{1}{\sqrt{\bar{\nu}_t}} z_t - \sqrt{\frac{1}{\bar{\nu}_t} - 1} \cdot \tanh(\sigma_\theta(z_t, t, s)), \quad (32)$$

where $\sigma_\theta(z_t, t, s)$ denotes a deep neural network parameterized by ϑ that predicts the denoising noise conditioned on the observed state s . To prevent excessive noise in the reconstructed decision z_0 , which may obscure the true action probabilities, the output is scaled using a hyperbolic tangent activation to ensure bounded noise levels.

During the reverse denoising process, each step t introduces a new noise component σ_ϑ , which remains independent of the forward-process noise σ . As a result, z_0 cannot be directly recovered using (32). Instead, we substitute (32) into the reverse transition expression in (31) to estimate the mean, shown as

$$\mu_\theta(z_t, t, s) = \frac{1}{\sqrt{\bar{\nu}_t}} \left(z_t - \frac{\varphi_t \tanh(\sigma_\vartheta(z_t, t, s))}{\sqrt{1 - \bar{\nu}_t}} \right). \quad (33)$$

We then sample z_{t-1} from the reverse transition distribution $p(z_t)p_\theta(z_{t-1}|z_t)$ and iterate this process over $t = T, T-1, \dots, 1$. By recursively applying these steps, the final generation distribution $p_\theta(z_0)$ is given by

$$p_\theta(z_0) = p(z_T) \prod_{t=1}^T p_\theta(z_{t-1}|z_t), \quad (34)$$

where $p(z_T)$ denotes a standard Gaussian distribution. After the reverse process yields the generative distribution $p_\theta(z_0)$, a sample of the final output z_0 can be drawn accordingly.

A common challenge in training generative models lies in the inability to backpropagate gradients through stochastic sampling operations. To overcome this, we adopt a reparameterization technique that separates the source of randomness from the distribution parameters. Specifically, the sampling is reformulated using the following update rule:

$$z_{t-1} = \mu_\theta(z_t, t, s) + (\tilde{\varphi}_t/2)^2 \odot \sigma, \quad (35)$$

where $\sigma \sim \mathcal{N}(\mathbf{0}, \mathbf{I})$. By recursively adopting the reverse update rule in (35), all intermediate states z_t ($0 \leq t \leq T$), including the final output z_0 , can be generated from an initial Gaussian noise sample.

Finally, the softmax function is applied to z_0 to convert it into a valid probability distribution, given by

$$\pi_{\vartheta}(s) = \left\{ \frac{e^{z_0^j}}{\sum_{i=1}^A e^{z_0^i}}, \forall j \in \mathcal{A} \right\} \quad (36)$$

Each element in $\pi_{\vartheta}(s)$ represents the probability of selecting a specific action under state s .

To implement the proposed approach in practice, the first step involves calculating the mean μ_{ϑ} of the reverse transition distribution $p_{\vartheta}(z_{t-1}|z_t)$, as defined in (29) and (33), and then update z_{t-1} using the rule in (35). Subsequently, the optimal decision distribution z_0 is obtained via (36). To further enhance optimization, we integrate the diffusion model into the Soft Actor-Critic (SAC) framework. SAC is an off-policy DRL algorithm that augments the reward with an entropy term to jointly maximize expected returns and policy entropy, effectively balancing exploration and exploitation.

3) *Experience Replay*: The agent continuously interacts with the environment to collect trajectory data. At slot n , the actor observes the state $s(n)$ and generates a discrete action distribution $\pi_{\vartheta}(s(n))$. An action $a(n) \sim \pi_{\vartheta}(s(n))$ is sampled and executed, after which the environment returns a reward $r(n) = (s(n), a(n))$ and transitions to the next state $s(n+1)$. The resulting transition tuple $(s(n), a(n), r(n), s(n+1))$ is stored in the experience replay buffer \mathcal{B} . This replay mechanism enables real-time interaction while allowing asynchronous sampling of past experiences, thereby enhancing training efficiency.

4) *Double Critic Networks*: In the proposed framework, the critic network is implemented as a soft Q-function $Q_{\psi}(s(n), a(n))$, which evaluates the expected return augmented by the entropy of the policy ψ under $(s(n), a(n))$. The formulation is given by

$$Q_{\psi}(s(n), a(n)) = E_{s(n+1) \sim \mathcal{B}}[r(s(n), a(n)) + \omega V_{\pi}(s(n+1))], \quad (37)$$

where ω denotes the reward discount factor, and $s(n+1)$ is the subsequent state sampled from the replay buffer \mathcal{B} . The corresponding soft value function $V_{\pi}(s(n))$ is expressed as:

$$V_{\pi}(s(n)) = E_{a(n) \sim \pi}[Q_{\psi}(s(n+1), a(n+1)) + \gamma J(\pi_{\vartheta}(s(n)))], \quad \text{s.t. } J(\pi_{\vartheta}(s(n))) = -\pi_{\vartheta}(s(n)) \log \pi_{\vartheta}(s(n)), \quad (38)$$

the term $J(\pi_{\vartheta}(s(n)))$ represents the entropy of the policy at state $s(n)$, while $\gamma \in [0, 1]$ is a tunable temperature coefficient that regulates the influence of the entropy in the objective. To reduce the overestimation bias often observed in Q-learning algorithms, GDRS incorporates a pair of critic networks, $Q_{\psi_1}(s(n), a(n))$ and $Q_{\psi_2}(s(n), a(n))$. The actor is trained using the smaller of the two Q-values, ensuring a conservative and stable policy update.

5) *Target Networks*: Each critic network is associated with a corresponding target network, parameterized by $\hat{\psi}_1$ and $\hat{\psi}_2$, respectively. These target networks mirror the architecture of their online counterparts and are introduced to enhance training stability by reducing fluctuations in target estimates.

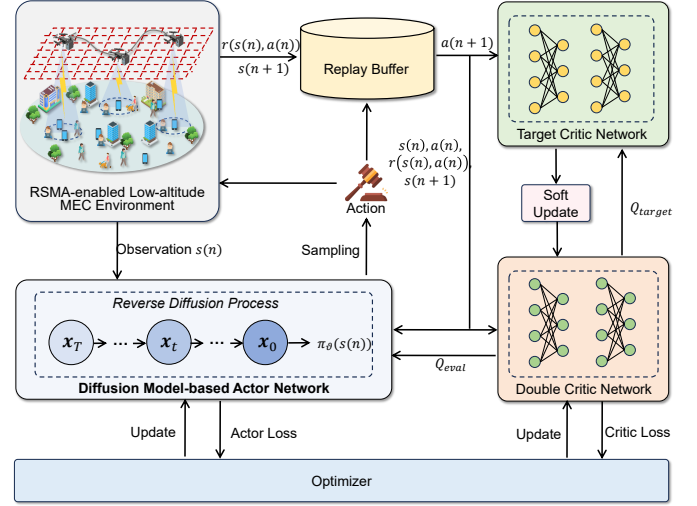


Fig. 2. The proposed GDRS optimization framework for joint optimization of UAV trajectory, task offloading and power allocation in RSMA-enabled low-altitude MEC systems.

To ensure smooth updates, their parameters are adjusted incrementally using a soft update strategy, defined as:

$$\hat{\psi}_i \leftarrow \varsigma \psi_i + (1 - \varsigma) \hat{\psi}_i, \quad (39)$$

where $\varsigma \in (0, 1]$ denotes the soft update rate, and $i = 1, 2$.

To train the critic networks, the agent draws a mini-batch of transition samples from the replay buffer \mathcal{B} and optimizes the network parameters by minimizing the following loss function:

$$L_Q(\psi_i) = E_{(s(n), a(n)) \sim \mathcal{B}} \left[\frac{1}{2} (Q_{\psi_i}(s(n), a(n)) - \hat{q})^2 \right], \quad (40)$$

where we define the Q-target \hat{q} as

$$\hat{q} = r(s(n), a(n)) + \omega V_{\hat{\psi}}(s(n+1)). \quad (41)$$

Subsequently, the parameters of the two critic networks are updated using gradient descent, following the update rule:

$$\psi_i \leftarrow \psi_i - \tau_c \nabla_{\psi_i} L_Q(\psi_i), \quad (42)$$

where τ_c represents the learning rate of the critic network for updating critic network parameters.

For training the policy network, the actor aims to maximize the expected Q-value to enhance decision-making quality. The objective function for updating the actor is defined as:

$$L_{\pi}(\vartheta) = E_{s(n) \sim \mathcal{B}} [\gamma J(\pi_{\vartheta}(s(n))) - \min_{i=1,2} Q_{\psi_i}(s(n), a(n))], \quad (43)$$

and we update the parameter ϑ , shown as

$$\vartheta \leftarrow \vartheta - \tau_a \nabla_{\vartheta} L_{\pi}(\vartheta), \quad (44)$$

where τ_a indicates the learning rate of actor network.

D. Algorithm Framework

Fig. 2 shows the framework of the proposed GDRS method, which extends the SAC algorithm. It comprises several core components for policy training, including an diffusion model-based actor network, double critic networks with corresponding target networks, an experience replay buffer, and the

Algorithm 1: GDRS: Generative Diffusion-Enhanced DRL for RSMA-enabled Low-Altitude MEC

Input: Initialize replay buffer \mathcal{B} ; actor parameters ϑ ; critic parameters ϕ_1, ϕ_2 ; target parameters $\hat{\psi}_1 \leftarrow \psi_1, \hat{\psi}_2 \leftarrow \psi_2$; training step index e ; diffusion step index t ; trajectory counter q .

```

1 while  $e < E$  do
2   while  $q < Q$  do
3     Determine the optimal decoding order  $\pi$ 
       according to Proposition 1;
4     Observe current state  $s(n)$ ; sample initial noise
        $z_T \sim \mathcal{N}(\mathbf{0}, \mathbf{I})$ ;
5     while  $t < T$  do
6       Apply denoising model  $\sigma_\vartheta(z_t, t, s(n))$ ;
7       Compute mean  $\mu_\vartheta$  and variance  $\tilde{\varphi}_t$  using
       (33) and (30);
8       Update  $z_t$  using (35);
9        $t \leftarrow t + 1$ ;
10    Sample discrete action  $a(n)$  to determine UAV
       trajectory, offloading, and power allocation;
11    Execute  $a(n)$  in the environment; record the
       resulting reward  $r(n)$  and the subsequent state
        $s'(n)$ ;
12    Store the transition tuple
        $(s(n), a(n), r(n), s'(n))$  in  $\mathcal{B}$ ;
13    Randomly select a mini-batch of samples from
        $\mathcal{B}$ ;
14    Update critic parameters  $\psi_1, \psi_2$  using (40),
       (42);
15    Update actor parameters  $\vartheta$  using (43) and (44);
16    Perform soft updates on  $\hat{\psi}_1, \hat{\psi}_2$  via (39);
17     $q \leftarrow q + 1$ ;
18   $e \leftarrow e + 1$ ;

```

Output: Optimized actor policy ϑ^* .

interaction environment [43]. In addition, the detailed progress of the proposed GDRS method is presented in Algorithm 1.

IV. SIMULATION RESULTS AND DISCUSSION

This section presents simulation studies designed to evaluate the effectiveness of the proposed GDRS approach. We begin by outlining the experimental configuration and baseline settings. Then, the simulation outcomes are discussed and examined thoroughly.

A. Experimental Setup

1) *Experimental Configuration:* We consider a task area measuring 1000×1000 m, which includes one UAV equipped with an MEC server and certain number of GTs. We set the initial location of the UAV as $[0, 0, 200]$. The total time slots of the system is set to 100, and each time slot is of length 1 s. According to the settings about propulsion model of the rotary-wing UAV [33], we set $U_t = 120$ m/s, $\bar{v} = 4.03$ m/s, $F_0 = 0.6$, $g = 0.05$, $\rho = 1.225$, $M = 0.503$. Each GT divides its transmitted signal into two distinct sub-messages,

TABLE I
SYSTEM PARAMETERS

Parameters	Values
Carrier frequency f_c	2.4 GHz
Environment constants α, β	12.08, 0.11 [34]
LoS and NLoS pathloss factors $\zeta_{\text{LoS}}, \zeta_{\text{NLoS}}$	1.6, 23 [44]
Communication bandwidth B	1 MHz
Maximum transmit power of each GT P_{\max}	5 mW
Speed of light c	3×10^8 m/s
Noise power N_0	-174 dBm/Hz
UAV flight time t_{\min}, t_{\max}	1 s, 5 s
UAV flight height h_{\min}, h_{\max}	100 m, 200 m
Maximum flight speed V_{\max}^h, V_{\max}^v	10 m/s, 10 m/s
Blade profile power W_0	79.9 W [33]
Induced power W_1	88.6 W [33]
Descending/ascending power W_2	11.46 W [33]
Processed rate of GT f_g	5 cycles/s
Processed rate of UAV f_u	100 ~ 500 cycles/s
The CPU cycles to be computed C_k	500 ~ 2500 bits
The amount of data to be processed D_k	1000 ~ 1500 cycles
Number of GTs K	2 ~ 5
Total time slots N	100
Minimal rate requirement R_{\min}	0.2 bit/s/Hz
The number of denoising steps T	10, 20, 30
Learning rate τ_c, τ_a	5×10^{-4}
Weight of soft update ς	0.005
Discount factor ω	0.95
Number of training episodes E	500
Batch size	64

i.e., $I = 2$. The rate-splitting ratio of the sub-messages is set to $\mu_{k,n,i} = 0.5, \forall k, n, i$. As for the training model, we set the learning rates of actor network and critic networks as $\tau_c = \tau_a = 5 \times 10^{-4}$, and set the update rate $\varsigma = 5 \times 10^{-3}$ for soft updating the target networks. All experiments were conducted in a Python 3.10 environment with PyTorch 2.1.0 on a server running Ubuntu, equipped with a 2.10 GHz Intel Xeon Gold 5218R processor (40 cores, 503 GB RAM) and an NVIDIA A100 GPU featuring 80 GB of memory. More parameters about the considered scenario and proposed method are shown in Table I.

2) *Baseline Settings:* To present fair comparison, we compare our proposed GDRS method with the following well-known DRL benchmark:

- PPORS: Proximal Policy Optimization for RSMA-enabled low-altitude MEC, where the agent learns an optimal policy in a discrete action space to maximize the energy efficiency.
- DQNRS: Deep Q-Network for RSMA-enabled low-altitude MEC, where the agent approximates the optimal action-value function in a discrete action space to maximize the energy efficiency.
- GDRS-Random: Generative diffusion-enhanced optimization for RSMA-enabled low-altitude MEC, where UAV adopts the random decoding order for uplink GTs instead of optimal policy proposed in **Proposition 1**.

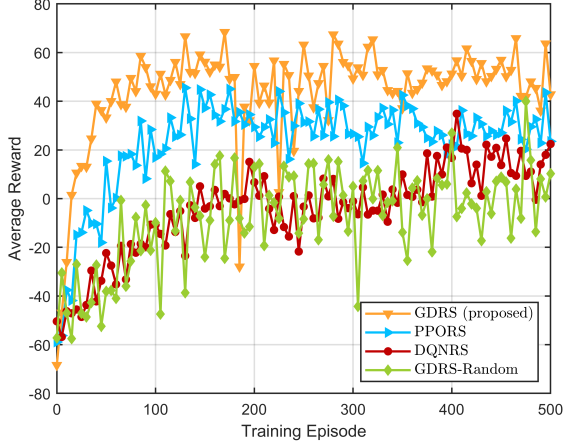


Fig. 3. The reward curves of the proposed GDRS algorithm and other baselines for RSMA-enabled LAE MEC systems over training episodes.

Additionally, in order to validate the effectiveness of the RSMA framework in supporting low-altitude MEC systems, we also design generative diffusion-enhanced algorithms under different multiple access schemes as baseline approaches:

- GDFD: Generative diffusion-enhanced optimization for Frequency Division Multiple Access (FDMA)-enabled low-altitude MEC, where the uplink bandwidth is equally divided among GTs, ensuring orthogonal transmissions without inter-user interference.
- GDNO: Generative diffusion-enhanced optimization for NOMA-enabled low-altitude MEC, where multiple GTs simultaneously share the same uplink resources via power-domain superposition coding and successive interference cancellation at the UAV.

B. Experimental Results

Fig. 3 plots the average reward obtained by GDRS and the baseline algorithms over training episodes. First, GDRS converges substantially faster and attains a higher steady-state reward than all baselines. Specifically, the reward curve of GDRS rises sharply and stabilizes at a high value after about 110 training episodes. Furthermore, the proposed GDRS method outperforms PPORS and DQNRS due to its enhanced exploration capability in high-dimensional hybrid action spaces, achieved by introducing a diffusion model to generate structured and high-quality action candidates. In addition, compared to the method with random decoding order, GDRS exhibits less fluctuation in its training curve and achieves a higher average reward, demonstrating the effectiveness of the optimized decoding order.

Fig. 4 examines the training reward curves of the proposed GDRS algorithm under different learning rates. When the learning rate is set to 5×10^{-4} , the training curve achieves higher reward values compared to those with learning rates of 1×10^{-4} and 1×10^{-3} . This is because a large learning rate causes excessively large update steps, resulting in unstable training for the agent. Conversely, a small learning rate leads to a slow learning process and causes the training to converge

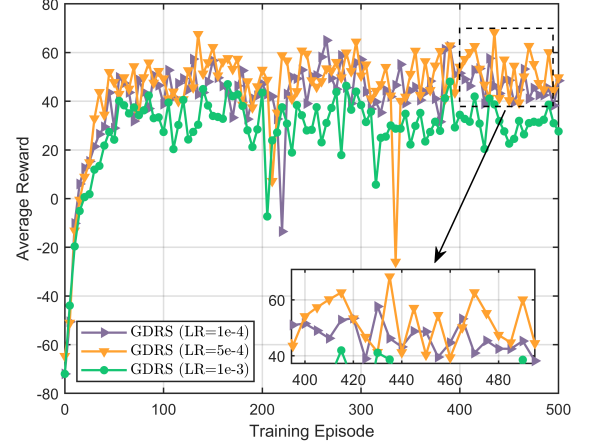


Fig. 4. The reward curves of the proposed GDRS algorithm under different learning rate.

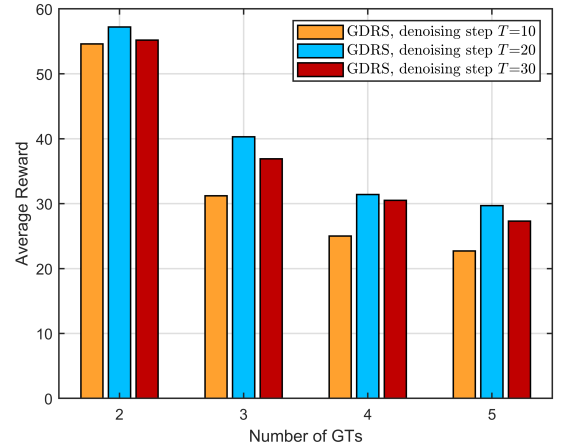


Fig. 5. The impact of diffusion steps T on average reward under different number of GTs K .

prematurely or get trapped in a local optimum. A learning rate of 5×10^{-4} strikes a better balance between learning stability and update efficiency. Therefore, all subsequent experiments adopt a learning rate of 5×10^{-4} .

Fig. 5 investigates how the number of diffusion steps T affects the achieved average reward under different numbers of GTs K . First, we observe that the GDRS method with 20 denoising steps outperforms the version with 10 denoising steps, indicating that increasing the number of denoising steps helps the DRL agent learn more generalizable features, thereby enhancing training generalization. However, the GDRS method with 30 denoising steps yields a significantly lower average reward compared to the 20-step case. This is because an excessive number of denoising steps can remove valuable features from the data, reducing training efficiency. Furthermore, as the number of GTs increases, the average reward under all denoising configurations decreases noticeably. This is due to the increased UAV flight energy consumption caused by the larger number of GTs under a fixed computational capacity, leading to reduced energy efficiency.

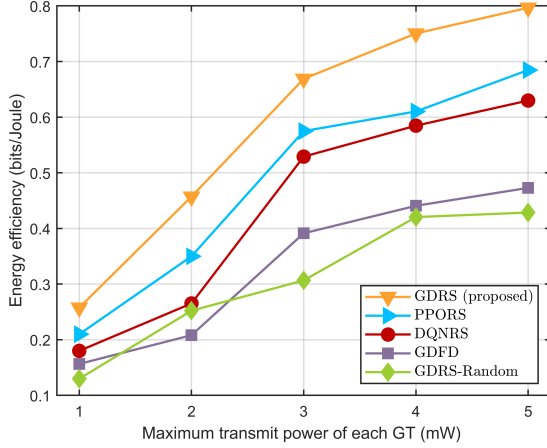


Fig. 6. Energy efficiency of different methods versus the maximum of transmit power of each GT.

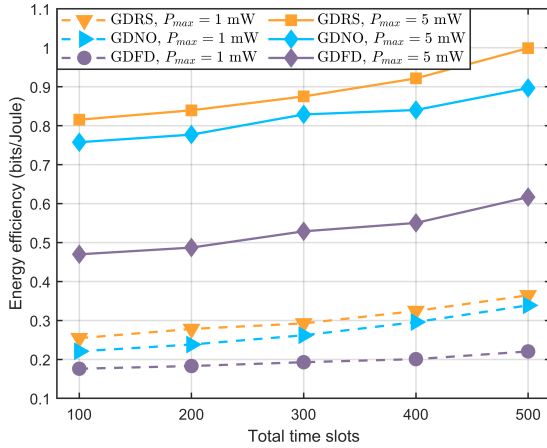


Fig. 7. Energy efficiency versus the total time slots of UAV under different multiple access methods.

Fig. 6 compares the energy efficiency of different methods versus the maximum transmit power of each GT. We find that all methods exhibit an upward trend as the maximum transmit power increases. This indicates that granting GTs higher transmit power generally enables more data bits to be offloaded and processed, and the growth in data bits outpaces the increase in UAV energy consumption. Moreover, we observe that the proposed GDRS method consistently achieves the highest energy efficiency across the entire power range, and the performance gap between GDRS and the baseline methods widens as the number of GTs increases. Additionally, we can observe that GDRS outperforms GDFD in terms of energy efficiency. This is because GDRS enables flexible interference management through successive interference cancellation, allowing simultaneous uplink transmissions over the shared bandwidth resource, whereas the GDFD method averages the bandwidth allocation, leading to reduced spectral efficiency and limited offloading performance.

Fig. 7 evaluates the energy efficiency versus the total number of time slots under different multiple access schemes.

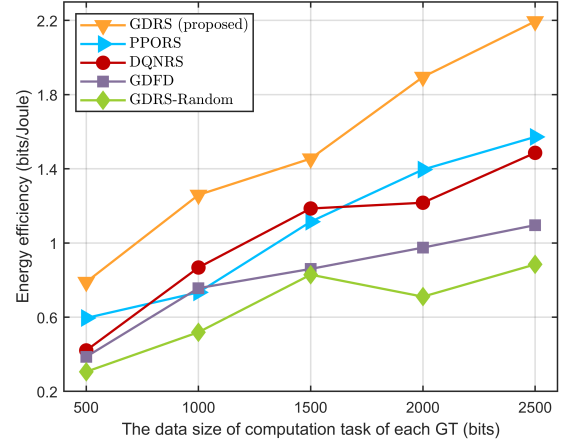


Fig. 8. Energy efficiency of different methods versus the data size of computation task of each GT.

We compare the proposed RSMA-based system with representative NOMA-based scheme and FDMA-based scheme. First, all schemes exhibit an increase in energy efficiency as the time horizon expands. Intuitively, with more time slots, the UAV has greater flexibility to serve the offloading requests in a staggered manner and can fly in a more energy-conservative trajectory, thereby improving the overall energy efficiency. Besides, the RSMA-enabled system achieves the highest energy efficiency, significantly outperforming both the NOMA and OMA cases. As the number of time slots increases, the energy efficiency gap widens because RSMA can more fully exploit the extra time to optimize power allocation and decoding order among users. Since it still allows concurrent transmissions with SIC, the NOMA-based system is generally second-best here, but it suffers from higher interference and less flexible rate allocation than RSMA, resulting in lower efficiency. The OMA method performs the worst energy-wise due to its poor spectral utilization. By enabling part of the interference to be treated as useful information, RSMA strikes an advantageous balance that NOMA and OMA cannot, thus delivering better performance especially in high-load or extended-duration scenarios.

In Fig. 8, we analyze how the energy efficiency of the various methods varies with the size of computation task of GT. The plotted results indicate a general upward trend in energy efficiency as the task size grows. When tasks are very small, the overhead of coordination and UAV operation is relatively significant, leading to lower energy efficiency for all schemes. In this regime, GDRS still maintains a slight edge over other methods, but overall efficiency is limited by fixed costs. As the task size increases, all methods become more energy-efficient. This is because larger batches of data can be offloaded and processed in one go, amortizing the energy cost of UAV trajectory and link setup over more bits. Notably, the energy efficiency of GDRS method improves the most rapidly and to the highest values. And the margin between GDRS and the others widens with task size, indicating that GDRS scales especially well to heavy workloads. This is because GDRS

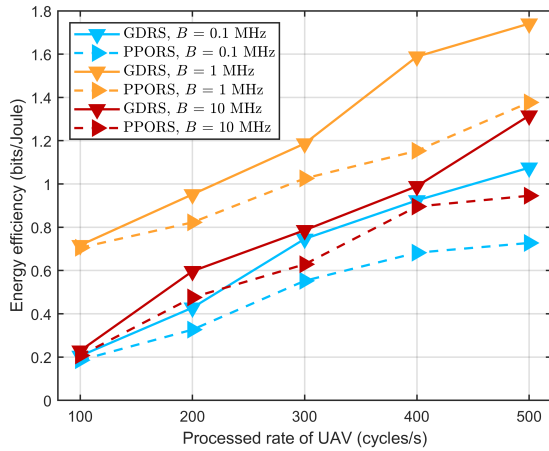


Fig. 9. Energy efficiency of GDRS and PPORS methods versus the processed rate of UAV under different communication bandwidth.

method minimizes unnecessary UAV movement and efficiently multiplexes the uplink transmissions via RSMA.

Fig. 9 plots the energy efficiency of GDRS versus the baseline PPORS against the processing rate of UAV under different bandwidth conditions. First, we observe that increasing the UAV's processing rate leads to higher energy efficiency for both GDRS and PPORS. With a faster onboard CPU, the UAV can execute offloaded tasks more quickly, reducing the time GTs spend transmitting. With a faster onboard CPU, the UAV can execute offloaded tasks more quickly, reducing the time GTs spend on data transmission. Moreover, the energy efficiency of GDRS consistently surpasses that of the PPORS method, demonstrating the advantage of the generative diffusion model in adapting to the complexity of low-altitude MEC offloading involving mobile UAV. In addition, under a fixed UAV processing rate, energy efficiency increases with communication bandwidth. When more bandwidth is available, uplink transmissions require less time or lower power for the same data volume, thereby improving the energy efficiency of both methods. Notably, even under constrained bandwidth conditions, GDRS outperforms the baseline. Specifically, when the UAV processing rate is set to 500 cycles/s and the bandwidth to 0.1 MHz, GDRS improves energy efficiency by approximately 47.3% compared to PPORS, confirming that whether the bottleneck lies in computation or communication, GDRS achieves better energy utilization.

Fig. 10 illustrates the UAV 3D trajectories under different methods. We observe that the proposed GDRS method yields a more structured and energy-aware trajectory that dynamically adapts to the spatial distribution of GTs, enabling efficient task offloading while minimizing redundant UAV motion. In contrast, the trajectories under PPORS and DQNRS exhibit erratic and less adaptive patterns, reflecting the limited exploration and poor generalization capability of traditional DRL approaches in high-dimensional hybrid action spaces. Additionally, the GDRS-Random method, which employs a stochastic RSMA decoding order, results in a degraded trajectory with inefficient hovering and detours, further highlighting the necessity of the decoding policy derived in Proposition 1.

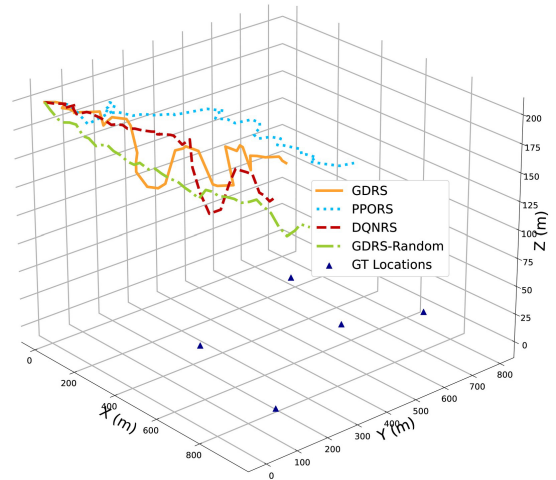


Fig. 10. UAV trajectories in 3D space for different methods.

V. CONCLUSION

In this paper, we investigated an uplink RSMA-enabled low-altitude MEC system to enhance energy efficiency under dynamic and interference-limited conditions. A novel generative diffusion model-enhanced DRL framework was proposed to jointly optimize UAV 3D trajectory, task offloading decisions, and power allocation. In addition, we analytically derive an optimal decoding order policy for the RSMA-enabled systems. Simulation results demonstrated that integrating RSMA with generative policy learning significantly improves energy efficiency and scalability in low-altitude MEC systems, particularly under dense user deployments and stringent resource constraints. Moreover, the diffusion model enhances policy exploration by generating structured actions that adapt to interference dynamics and user distributions, enabling more effective and energy-aware UAV behavior. However, this work assumes perfect knowledge of channel state information and GT locations, which may not be realistic in practical deployments. Therefore, future work will explore adaptive optimization schemes that are robust to imperfect channel conditions and mobile GT scenarios.

REFERENCES

- [1] E. Calvanese Strinati, S. Barbarossa, J. L. Gonzalez-Jimenez, D. Ktenas, N. Cassiau, L. Maret, and C. Dehos, "6G: The Next Frontier: From Holographic Messaging to Artificial Intelligence Using Subterahertz and Visible Light Communication," *IEEE Vehicular Technology Magazine*, vol. 14, no. 3, pp. 42–50, 2019.
- [2] P. Porambage, J. Okwuibe, M. Liyanage, M. Ylianttila, and T. Taleb, "Survey on Multi-Access Edge Computing for Internet of Things Realization," *IEEE Communications Surveys & Tutorials*, vol. 20, no. 4, pp. 2961–2991, 2018.
- [3] L. Nadeem, M. A. Azam, Y. Amin, M. A. Al-Ghamdi, K. K. Chai, M. F. N. Khan, and M. A. Khan, "Integration of D2D, Network Slicing, and MEC in 5G Cellular Networks: Survey and Challenges," *IEEE Access*, vol. 9, pp. 37 590–37 612, 2021.
- [4] Y. Jiang, X. Li, G. Zhu, H. Li, J. Deng, K. Han, C. Shen, Q. Shi, and R. Zhang, "Integrated Sensing and Communication for Low Altitude Economy: Opportunities and Challenges," *IEEE Communications Magazine*, pp. 1–7, 2025.
- [5] C. Zhao, J. Wang, R. Zhang, D. Niyato, G. Sun, H. Du, D. I. Kim, and A. Jamalipour, "Generative AI-enabled Wireless Communications for Robust Low-altitude Economy Networking," *arXiv preprint arXiv:2502.18118*, 2025.

- [6] S. Jeong, O. Simeone, and J. Kang, "Mobile Edge Computing via a UAV-Mounted Cloudlet: Optimization of Bit Allocation and Path Planning," *IEEE Transactions on Vehicular Technology*, vol. 67, no. 3, pp. 2049–2063, 2018.
- [7] Y. Mao, O. Dizdar, B. Clerckx, R. Schober, P. Popovski, and H. V. Poor, "Rate-Splitting Multiple Access: Fundamentals, Survey, and Future Research Trends," *IEEE Communications Surveys & Tutorials*, vol. 24, no. 4, pp. 2073–2126, 2022.
- [8] X. Wang, H. Du, L. Feng, D. Niyato, F. Zhou, Z. Yang, and W. Li, "Resource Allocation and User Pairing for Rate Splitting Multiple Access Based Wireless Networked Control Systems," *IEEE Transactions on Communications*, pp. 1–1, 2024.
- [9] H. Bastami, H. Behroozi, M. Moradikia, A. Abdelhadi, D. W. K. Ng, and L. Hanzo, "Large-Scale Rate-Splitting Multiple Access in Uplink UAV Networks: Effective Secrecy Throughput Maximization Under Limited Feedback Channel," *IEEE Transactions on Vehicular Technology*, vol. 72, no. 7, pp. 9267–9280, 2023.
- [10] C. Zhang, G. Sun, J. Li, Q. Wu, J. Wang, D. Niyato, and Y. Liu, "Multi-Objective Aerial Collaborative Secure Communication Optimization via Generative Diffusion Model-Enabled Deep Reinforcement Learning," *IEEE Transactions on Mobile Computing*, vol. 24, no. 4, pp. 3041–3058, 2025.
- [11] C. Fang, Z. Hu, X. Meng, S. Tu, Z. Wang, D. Zeng, W. Ni, S. Guo, and Z. Han, "DRL-Driven Joint Task Offloading and Resource Allocation for Energy-Efficient Content Delivery in Cloud-Edge Cooperation Networks," *IEEE Transactions on Vehicular Technology*, vol. 72, no. 12, pp. 16 195–16 207, 2023.
- [12] F. You and H. Du, "ReaCritic: Large Reasoning Transformer-based DRL Critic-model Scaling For Heterogeneous Networks," *arXiv preprint arXiv:2505.10992*, 2025.
- [13] H. Du, R. Zhang, Y. Liu, J. Wang, Y. Lin, Z. Li, D. Niyato, J. Kang, Z. Xiong, S. Cui, B. Ai, H. Zhou, and D. I. Kim, "Enhancing Deep Reinforcement Learning: A Tutorial on Generative Diffusion Models in Network Optimization," *IEEE Communications Surveys & Tutorials*, vol. 26, no. 4, pp. 2611–2646, 2024.
- [14] X. Wang, H. Du, D. Niyato, L. Zhou, L. Feng, Z. Yang, F. Zhou, and W. Li, "Generative AI Enabled Matching for 6G Multiple Access," *arXiv preprint arXiv:2411.04137*, 2024.
- [15] X. Xu, X. Mu, Y. Liu, H. Xing, Y. Liu, and A. Nallanathan, "Generative Artificial Intelligence for Mobile Communications: A Diffusion Model Perspective," *IEEE Communications Magazine*, pp. 1–8, 2024.
- [16] F. You, H. Du, X. Hou, Y. Ren, and K. Huang, "DRESS: Diffusion Reasoning-based Reward Shaping Scheme For Intelligent Networks," *arXiv preprint arXiv:2503.07433*, 2025.
- [17] Z. Yang, S. Bi, and Y.-J. A. Zhang, "Dynamic Offloading and Trajectory Control for UAV-Enabled Mobile Edge Computing System With Energy Harvesting Devices," *IEEE Transactions on Wireless Communications*, vol. 21, no. 12, pp. 10 515–10 528, 2022.
- [18] Z. Hu, F. Zeng, Z. Xiao, B. Fu, H. Jiang, and H. Chen, "Computation Efficiency Maximization and QoE-Provisioning in UAV-Enabled MEC Communication Systems," *IEEE Transactions on Network Science and Engineering*, vol. 8, no. 2, pp. 1630–1645, 2021.
- [19] B. Liu, Y. Wan, F. Zhou, Q. Wu, and R. Q. Hu, "Resource Allocation and Trajectory Design for MISO UAV-Assisted MEC Networks," *IEEE Transactions on Vehicular Technology*, vol. 71, no. 5, pp. 4933–4948, 2022.
- [20] Y. Wang, J. Zhu, H. Huang, and F. Xiao, "Bi-Objective Ant Colony Optimization for Trajectory Planning and Task Offloading in UAV-Assisted MEC Systems," *IEEE Transactions on Mobile Computing*, vol. 23, no. 12, pp. 12 360–12 377, 2024.
- [21] J. Feng, X. Liu, Z. Liu, and T. S. Durrani, "Optimal Trajectory and Resource Allocation for RSMA-UAV Assisted IoT Communications," *IEEE Transactions on Vehicular Technology*, vol. 73, no. 6, pp. 8693–8704, 2024.
- [22] H. Bastami, M. Letafati, M. Moradikia, A. Abdelhadi, H. Behroozi, and L. Hanzo, "On the Physical Layer Security of the Cooperative Rate-Splitting-Aided Downlink in UAV Networks," *IEEE Transactions on Information Forensics and Security*, vol. 16, pp. 5018–5033, 2021.
- [23] R. Han, Y. Wen, L. Bai, J. Liu, and J. Choi, "Rate Splitting on Mobile Edge Computing for UAV-Aided IoT Systems," *IEEE Transactions on Cognitive Communications and Networking*, vol. 6, no. 4, pp. 1193–1203, 2020.
- [24] Q. Zhou, Y. Liu, H. Feng, and L. Wang, "PRU Group Allocation and Dynamic Rate-splitting Design for Power Minimization in IRS-assisted UAV MEC Systems With RSMA," *IEEE Transactions on Green Communications and Networking*, pp. 1–1, 2024.
- [25] J. Kim, E. Hong, J. Jung, J. Kang, and S. Jeong, "Energy Minimization in Reconfigurable Intelligent Surface-assisted Unmanned Aerial Vehicle-enabled Wireless Powered Mobile Edge Computing Systems with Rate-splitting Multiple Access," *Drones*, vol. 7, no. 12, p. 688, 2023.
- [26] J. Chen, X. Cao, P. Yang, M. Xiao, S. Ren, Z. Zhao, and D. O. Wu, "Deep Reinforcement Learning Based Resource Allocation in Multi-UAV-Aided MEC Networks," *IEEE Transactions on Communications*, vol. 71, no. 1, pp. 296–309, 2023.
- [27] J. Liu, M. Xiao, J. Wen, J. Kang, R. Zhang, T. Zhang, D. Niyato, W. Zhang, and Y. Liu, "Optimizing Resource Allocation for Multi-Modal Semantic Communication in Mobile AIGC Networks: A Diffusion-Based Game Approach," *IEEE Transactions on Cognitive Communications and Networking*, pp. 1–1, 2025.
- [28] C. Zhao, R. Zhang, J. Wang, D. Niyato, G. Sun, H. Du, Z. Li, A. Jamalipour, and D. I. Kim, "Temporal Spectrum Cartography in Low-Altitude Economy Networks: A Generative AI Framework with Multi-Agent Learning," *arXiv preprint arXiv:2505.15571*, 2025.
- [29] X. Zhang and J. Yu, "Improve the Training Efficiency of DRL for Wireless Communication Resource Allocation: The Role of Generative Diffusion Models," *arXiv preprint arXiv:2502.07211*, 2025.
- [30] X. Wang, H. Du, L. Feng, F. Zhou, and W. Li, "Effective Throughput Maximization for NOMA-Enabled URLLC Transmission in Industrial IoT Systems: A Generative AI-Based Approach," *IEEE Internet of Things Journal*, vol. 12, no. 10, pp. 13 327–13 339, 2025.
- [31] J. Zhang, Z. Liu, X. Feng, H. Yang, and S. Liang, "Enhanced Secure Beamforming for IRS-Assisted IoT Communication Using a Generative-Diffusion-Model-Enabled Optimization Approach," *IEEE Internet of Things Journal*, vol. 12, no. 10, pp. 13 398–13 414, 2025.
- [32] J. Wang, H. Du, D. Niyato, J. Kang, Z. Xiong, D. Rajan, S. Mao, and X. Shen, "A Unified Framework for Guiding Generative AI With Wireless Perception in Resource Constrained Mobile Edge Networks," *IEEE Transactions on Mobile Computing*, vol. 23, no. 11, pp. 10 344–10 360, 2024.
- [33] H. Mei, K. Wang, D. Zhou, and K. Yang, "Joint Trajectory-Task-Cache Optimization in UAV-Enabled Mobile Edge Networks for Cyber-Physical System," *IEEE Access*, vol. 7, pp. 156 476–156 488, 2019.
- [34] A. Al-Hourani, S. Kandeepan, and S. Lardner, "Optimal LAP Altitude for Maximum Coverage," *IEEE Wireless Communications Letters*, vol. 3, no. 6, pp. 569–572, 2014.
- [35] Y. Du, K. Wang, K. Yang, and G. Zhang, "Energy-Efficient Resource Allocation in UAV Based MEC System for IoT Devices," in *2018 IEEE Global Communications Conference (GLOBECOM)*, 2018, pp. 1–6.
- [36] Z. Yang, M. Chen, W. Saad, W. Xu, and M. Shikh-Bahaei, "Sum-Rate Maximization of Uplink Rate Splitting Multiple Access (RSMA) Communication," *IEEE Transactions on Mobile Computing*, vol. 21, no. 7, pp. 2596–2609, 2022.
- [37] J. Zhu, Y. Huang, J. Wang, K. Navaie, and Z. Ding, "Power Efficient IRS-Assisted NOMA," *IEEE Transactions on Communications*, vol. 69, no. 2, pp. 900–913, 2021.
- [38] M. Zeng, X. Li, G. Li, W. Hao, and O. A. Dobre, "Sum Rate Maximization for IRS-Assisted Uplink NOMA," *IEEE Communications Letters*, vol. 25, no. 1, pp. 234–238, 2021.
- [39] J. Zhang, L. Zhu, Z. Xiao, X. Cao, D. O. Wu, and X.-G. Xia, "Optimal and Sub-Optimal Uplink NOMA: Joint User Grouping, Decoding Order, and Power Control," *IEEE Wireless Communications Letters*, vol. 9, no. 2, pp. 254–257, 2020.
- [40] M. A. Abd-Elmagid, A. Ferdowsi, H. S. Dhillon, and W. Saad, "Deep Reinforcement Learning for Minimizing Age-of-Information in UAV-Assisted Networks," in *2019 IEEE Global Communications Conference (GLOBECOM)*, 2019, pp. 1–6.
- [41] A. Q. Nichol and P. Dhariwal, "Improved Denoising Diffusion Probabilistic Models," in *International conference on machine learning*, PMLR, 2021, pp. 8162–8171.
- [42] "Denoising Diffusion Probabilistic Models, author=Ho, Jonathan and Jain, Ajay and Abbeel, Pieter," *Advances in neural information processing systems*, vol. 33, pp. 6840–6851, 2020.
- [43] H. Du, Z. Li, D. Niyato, J. Kang, Z. Xiong, H. Huang, and S. Mao, "Diffusion-Based Reinforcement Learning for Edge-Enabled AI-Generated Content Services," *IEEE Transactions on Mobile Computing*, vol. 23, no. 9, pp. 8902–8918, 2024.
- [44] Y. Zhao, F. Zhou, L. Feng, Y. Sun, W. Li, W. Y. B. Lim, Z. Xiong, S. Mao, and Z. Han, "Joint Deployment and Resource Allocation for Multi-AeBS Networks: A Two-Timescale Optimization Framework Using MADRL," *IEEE Transactions on Communications*, pp. 1–1, 2024.